

Extreme thermodynamics in nanolitre volumes through stimulated Brillouin–Mandelstam scattering

Received: 8 August 2022

Accepted: 7 August 2023

Published online: 25 September 2023

 Check for updates

Andreas Geilen^{1,2,8}, Alexandra Popp^{1,2,3,8}, Debayan Das^{1,4}, Saher Junaid⁵, Christopher G. Poulton⁶, Mario Chemnitz⁷, Christoph Marquardt^{1,2,3}, Markus A. Schmidt^{5,7} & Birgit Stiller^{1,2,3} ✉

Examining the physical properties of materials—particularly of toxic liquids—under a wide range of thermodynamic states is a challenging problem due to the extreme conditions the material has to experience. Such temperature and pressure regimes, which result in a change in the refractive index and sound velocity, can be accessed by optoacoustic interactions such as Brillouin–Mandelstam scattering. Here we demonstrate the Brillouin–Mandelstam measurements of nanolitre volumes of liquids in extreme thermodynamic regimes. This is enabled by a fully sealed liquid-core optical fibre containing carbon disulfide. Within this waveguide, which exhibits tight optoacoustic confinement and a high Brillouin gain, we are able to conduct spatially resolved measurements of the local Brillouin response, giving us access to a resolved image of the temperature and pressure values along the liquid channel. We measure the material properties of the liquid core at very large positive pressures (above 1,000 bar) and substantial negative pressures (below –300 bar), as well as explore the isobaric and isochoric regimes. The extensive thermodynamic control allows the tunability of the Brillouin frequency shift of more than 40% using only minute volumes of liquid.

Understanding the physics at extreme thermodynamic points such as high pressures or high temperatures has been challenging for several decades^{1,2}. An illustrative example is the exploration of the negative-pressure regime that has vast implications for the understanding of diffusion processes in the micro- and nanoscopic world, being particularly relevant for mineral transport in plants³ and body cells⁴, as well as for potential advances in material engineering⁵. The lack of reconfigurable and reproducible measurement schemes at negative pressures has caused debates about the phase diagram of water up

to our modern age⁶ and has not let much room for generalizing the negative-pressure concept to molecular systems other than water to date. In general, the experimental study of liquids under extreme conditions can be exceptionally demanding due to the need for thermodynamic stabilization⁷ and the handling of liquids⁸, particularly when the liquids involved pose risks to health and the environment.

Non-contact measurements that encapsulate the material of interest from the environment are, therefore, highly desirable and can be performed by measuring optical^{9–11} or acoustic^{12–14} parameters of the

¹Max Planck Institute for the Science of Light, Erlangen, Germany. ²Department of Physics, Friedrich-Alexander Universität Erlangen-Nürnberg, Erlangen, Germany. ³SAOT, Graduate School in Advanced Optical Technologies, Erlangen, Germany. ⁴Université Bourgogne France-Comté, Besançon, France. ⁵Leibniz Institute of Photonic Technology, Jena, Germany. ⁶School of Mathematical and Physical Sciences, University of Technology Sydney, Sydney, New South Wales, Australia. ⁷Otto Schott Institute of Materials Research (OSIM), Jena, Germany. ⁸These authors contributed equally: Andreas Geilen, Alexandra Popp. ✉e-mail: birgit.stiller@mpl.mpg.de

material. In particular, combining the advantages of both optics and acoustics via stimulated Brillouin–Mandelstam scattering (SBS)—a nonlinear interaction of light and sound waves—allows to probe changes in temperature, pressure and density with high precision. SBS has been demonstrated in liquids¹⁵, gases¹⁶ and optical fibres¹⁷. In particular, optical fibres are a very common platform for SBS applications such as microwave photonics¹⁸, signal processing^{19–21} and sensing²² because of their low optical loss, long interaction lengths, easy handling and tight optoacoustic confinement.

However, the use of conventional glass materials in optical fibres prevents the platform to unfold its potential for material studies. Using liquids as a guiding core medium opens up this potential by providing access to the thermodynamics of fluids and reducing sample amounts to nanolitre volumes and preserving the metre-long interaction lengths and high field confinement of optical fibres. Such liquid-core optical fibres (LiCOFs) have already found applications in supercontinuum generation²³, lasing²⁴, temperature sensing²⁵ or signal processing²⁶. Also, first experiments of SBS in open LiCOFs have been performed²⁷. Yet, access to extreme thermodynamic ranges of liquids, such as very high or even negative pressures, has so far been beyond reach with fibre optics. Moreover, the full description of such dynamics requires a method sensitive to thermodynamic parameters like the refractive index and speed of sound, ideally spatially resolved along the fibre axis. Here SBS provides both by exploiting the interaction of optical and acoustic waves.

In this work, we present an optoacoustic, fully fibre-integrated photonic platform that allows access to extreme thermodynamic regimes of liquid materials. This framework exploits SBS in fully sealed and low-loss LiCOFs with unprecedented capabilities to sense temperature and pressure dynamics of liquids in a spatially resolved and highly reproducible fashion within a waveguide environment that simultaneously confines light and sound. We demonstrate our concept using only a few nanolitres of volatile and toxic carbon disulfide (CS₂) in an experimental case study.

Our all-fibre setup allows for the local and global control of the thermodynamic state of CS₂. The characterization of the optoacoustic response reveals a substantial Brillouin gain of $(32.2 \pm 0.8) \text{ W}^{-1} \text{ m}^{-1}$. In particular, we perform spatially resolved measurements of the optoacoustic interaction using Brillouin optical correlation domain analysis (BOCDA) with centimetre resolution. This investigation allows us to determine the local and global influences of temperature and pressure changes.

Our framework allows us to probe up to pressure values larger than 1,000 bar and unprecedented negative pressures down to -300 bar. With these insights, we are able to perform the thermodynamic control of SBS, allowing us to tailor the Brillouin frequency shift (BFS) by more than 40% of its initial value with high precision. We extend our measurements from the isochoric (constant volume) to the isobaric (constant pressure) regime of the liquid. Studying the latter, we show that the absence of the pressure component leads to a more than sevenfold enhancement in temperature sensitivity of the BFS compared with standard solid-core fibres. In this case, SBS is extremely well suited, since the air gap formation inside the fibre prevents any transmission measurements. Additionally, the isochoric state at the boundary to the isobaric state allows stable and reproducible access to the regime of negative pressure. This metastable state is associated with a stretched liquid, where attractive forces between the molecules prevent the formation of an energetically more favourable state of separated liquid and gas phase²⁸. This regime is normally only accessible with high experimental expenses and has rarely been achieved in liquids other than water and at such high negative-pressure values²⁹. Indeed, probing those boundaries of metastable thermodynamic regimes is of particular importance for verifying the equations of states in common molecular models³⁰. Our work uniquely showcases the use of optoacoustics as a tool for material sciences to advance our

understanding of thermodynamics as well as the potential to implement highly sensitive fibre sensors, chemical nanoreactors and tunable radio-frequency filters. This work might open a new area where scarce quantities of material can be investigated at points in the phase diagram that were hard to reach before with an optoacoustics-based method that is especially sensitive to the environment.

Brillouin–Mandelstam scattering in CS₂-filled LiCOF

Brillouin–Mandelstam scattering is an optoacoustic effect where a strong pump laser is coherently scattered by travelling acoustic waves, resulting in a backscattered Stokes and anti-Stokes signal. The Stokes signal is frequency downshifted by the BFS $\Omega_B/2\pi$ and shows a Lorentzian shape. A comprehensive tutorial on Brillouin scattering can be found elsewhere³¹. The BFS is described as

$$\frac{\Omega_B}{2\pi} = \frac{2}{\lambda} \times n_{\text{eff}}(p, T) \times v_{\text{ac}}(p, T), \quad (1)$$

where both speed of sound $v_{\text{ac}}(p, T)$ and mode refractive index $n_{\text{eff}}(p, T)$ are dependent on temperature T and pressure p inside the fibre³². In contrast to solid-core fibres, in LiCOFs, externally applied local stresses distribute throughout the core in the form of changes in global pressure. Indeed, due to the fluid state of the core material, the pressure can be assumed to be constant along the fibre as a potential pressure gradient is eventually equalized through the flow. In contrast, the temperature is a local property ($T = T(z)$) as a change in temperature at location $z = z_1$ does not impose the temperature to change at $z = z_2$. For the mode refractive index, we use the extended Sellmeier equation²⁶ to describe pressure and temperature dependencies. We assume that the speed of sound can be separately described by a linear combination of contributions from the pressure and temperature, with the pressure contribution taken from the model in ref. 25 and the temperature contribution from that in ref. 33. In this case, $n(\text{CS}_2, 1 \text{ bar}, 20 \text{ }^\circ\text{C}) = 1.588$ is the refractive index and $v_{\text{ac}}(\text{CS}_2, 1 \text{ bar}, 20 \text{ }^\circ\text{C}) = 1,242 \text{ m s}^{-1}$ is the speed of sound for CS₂.

In our experimental system, liquid CS₂ is sealed within a fused silica capillary by direct hot splicing to glass fibres. The high-index core liquid embedded in the lower-index silica forms a close-to-ideal circular step-index optical and acoustic waveguide, whereas the fibre has been engineered for efficient coupling to standard single-mode fibre (SMF) pigtailed via bridge fibres (Methods).

Controlling the temperature in the capillary can be straightforwardly done by external heating or cooling, but directly controlling the pressure is more involved. An increase in temperature leads to the expansion of CS₂, following $\frac{1}{L} \left(\frac{\partial L}{\partial T} \right)_p = \alpha_v$, where $\alpha_v = 1.12 \times 10^{-3} \text{ K}^{-1}$ is the volumetric coefficient of expansion of CS₂ at 20 °C (ref. 34). If the liquid fills the complete capillary, it cannot expand further, which then translates to an increase in pressure. Following another work⁴¹ and extending it for partially heated fibres, the relation between a temperature change and a pressure change is determined by

$$\Delta p = \frac{\alpha_v}{\kappa} \frac{L_H}{L} \Delta T, \quad (2)$$

where $\kappa = 9.38 \times 10^{-10} \text{ Pa}^{-1}$ is the isothermal compressibility of CS₂ (ref. 34) and L_H is the heated length, assuming $\alpha_v \Delta T \ll 1$. With this relation, T being a local property and p being a global property of CS₂, one can change the pressure in the complete LiCOF by heating one part of the fibre, which does not change the temperature of the other part. In contrast to non-sealed systems^{35,36}, this relation provides full control of the pressure without requiring open access to the liquid, by partially heating or cooling the fibre and keeping the temperature of the other region constant.

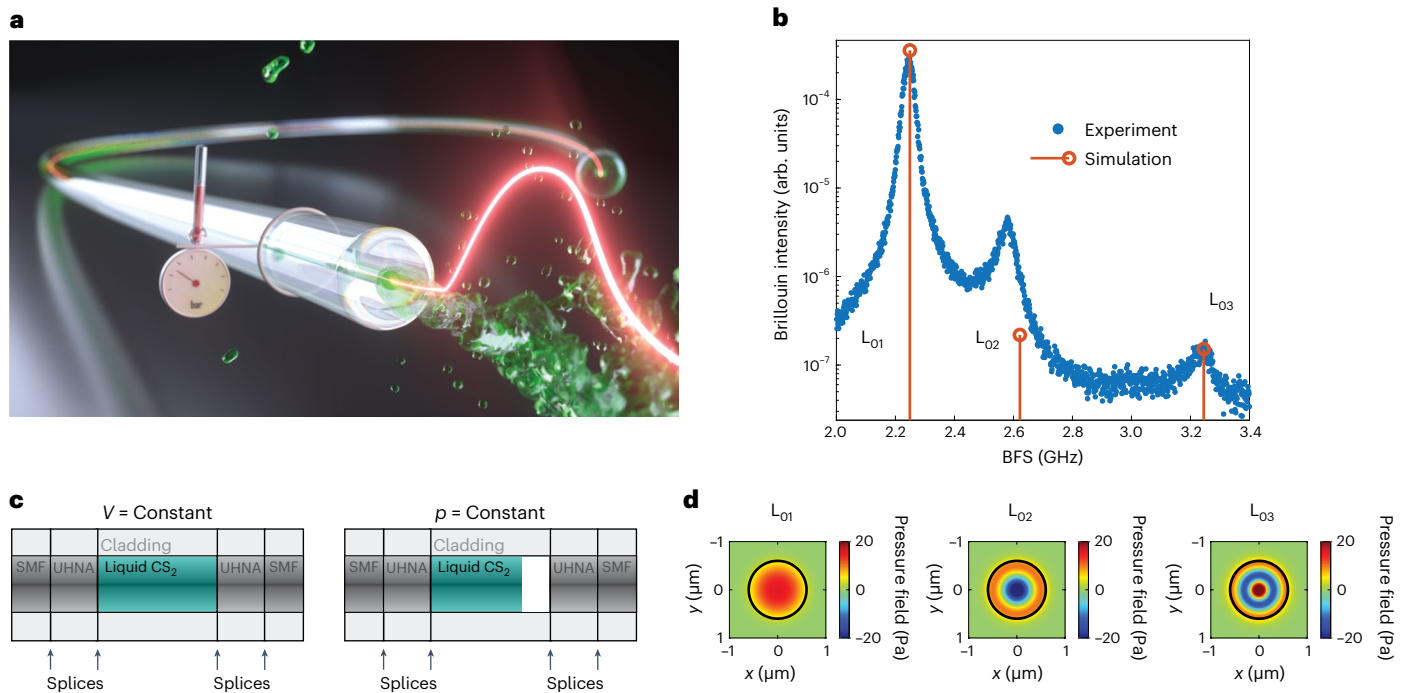


Fig. 1 | Sample geometry and analysis of the integrated Brillouin spectrum at room temperature. **a**, Artist's view of the LiCOF sample with a laser. **b**, Measured spectrum (blue) and simulation (red) of SBS spectrum with 1.125 μm core diameter. **c**, Geometry of the LiCOF sample spliced on both sides with a UHNA fibre for coupling and sealing. SMF is used for integrability. If the capillary

is fully filled, the volume (V) stays constant (isochoric regime), whereas if a bubble is present, the pressure (P) stays constant (isobaric regime). **d**, Numerical simulations of the corresponding longitudinal, radially symmetric pressure acoustic modes L_{01} , L_{02} and L_{03} . Panel **a** credit: Long Huy Dao.

To illustrate the thermodynamic behaviour of this system, a schematic of the LiCOF geometry is shown in Fig. 1c. Two regimes are depicted in Fig. 1c: first, the isochoric regime, in which the fibre is fully filled and the CS_2 volume is constant (left). In this regime, the fibre has optical transmission and an increase in temperature also increases the internal pressure. Second, the isobaric regime, where a gap is present and the pressure in CS_2 is constant (right). In this regime, the fibre does not transmit light but is accessible via backward SBS from one side.

Integrated Brillouin–Mandelstam analysis

To gain a fundamental understanding of the Brillouin–Mandelstam response of the LiCOF, we perform an integrated, thermally seeded SBS analysis at a pump wavelength of $\lambda = 1,549 \text{ nm}$. Extended Data Fig. 1 shows a simplified sketch of the setup. The SBS spectrum at room temperature is shown in Fig. 1b, where we observe peaks at 2.25, 2.58 and 3.24 GHz. Numerical simulations reveal that the peaks are due to high optoacoustic overlap between the fundamental optical mode and the first three radially symmetric longitudinal-pressure acoustic modes, namely, L_{01} , L_{02} and L_{03} (Fig. 1d), with BFSs at 2.25, 2.62 and 3.24 GHz, respectively. Therefore, the simulations qualitatively confirm the origin of the rich mode spectrum due to multiple acoustic modes only, in the absence of higher-order optical modes. We find a small deviation in the BFS of the second peak from the simulated value, which is probably due to the idealized geometry of the capillary in the numerical model. It should be noted that the simulation uses the refractive index $n(\text{CS}_2, p = 1 \text{ bar}, T = 20^\circ\text{C}) = 1.588$ and the speed of sound $v_{\text{ac}}(\text{CS}_2, p = 1 \text{ bar}, T = 20^\circ\text{C}) = 1,242 \text{ ms}^{-1}$. For the peak at 2.25 GHz, we find a total gain of $(9.29 \pm 0.23) \text{ W}^{-1} \text{ m}^{-1}$, and a gain of $(32.2 \pm 0.8) \text{ W}^{-1} \text{ m}^{-1}$ when compensating for the coupling losses of 5.4 dB with a linewidth of 65 MHz. This value is two orders of magnitude higher than the values of a standard SMF at around $(0.2\text{--}0.3) \text{ W}^{-1} \text{ m}^{-1}$ (refs. 37,38). Supplementary Section 1 provides a detailed description of how the gain is measured, whereas the underlying physics is comprehensively described elsewhere^{17,31}.

In Fig. 2a, the temperature response of the LiCOF is investigated by measuring the Brillouin spectrum and heating a part of the capillary from room temperature to 130 $^\circ\text{C}$ in steps of 5 $^\circ\text{C}$ on a hotplate. Above room temperature, the peaks associated with the first- and second-order longitudinal-pressure acoustic modes split up and move to higher frequencies with increasing temperature. To identify the peaks in the following, we number them from 1 to 4 by increasing the frequency. The observed splitting is explained in Fig. 2b by the additive but opposite influence of global pressure (positive) and local temperature (negative) via the thermo- and piezo-optic coefficients of CS_2 . First, the global pressure influence, following equation (2), upshifts the BFS inside and along the whole core (Fig. 2b, green solid arrows). Second, the local temperature influence downshifts the BFS only in the heated part of the capillary relative to the upshifted one (Fig. 2b, red dashed arrows). In the integrated spectrum, the local Brillouin spectra along the whole fibre are summed up¹⁷, resulting in the observed splitting (Fig. 2a). We can now identify each peak with the influences it is subjected to: although all the four peaks are subjected to a BFS upshift due to pressure changes (green arrows marked with green circles), only peaks 1 and 3 are subject to an additional BFS downshift due to temperature changes (red arrows marked with circles having a red–green gradient), as shown in Fig. 2b. This allows us to discriminate the influences of both temperature and pressure.

Spatially resolved Brillouin–Mandelstam analysis

To experimentally confirm the local and global nature of the pressure and temperature influence on the different peaks, we employ direct-frequency-modulated BOCDA^{39,40} for a distributed analysis of the fibre. Extended Data Fig. 2 shows a sketch of the setup. Following the scheme shown in Fig. 3a, a frequency-modulated, counterpropagating pump in combination with a probe creates a localized acoustic response inside the fibre. By changing the frequency of the modulation, the correlation position can be moved throughout the fibre to

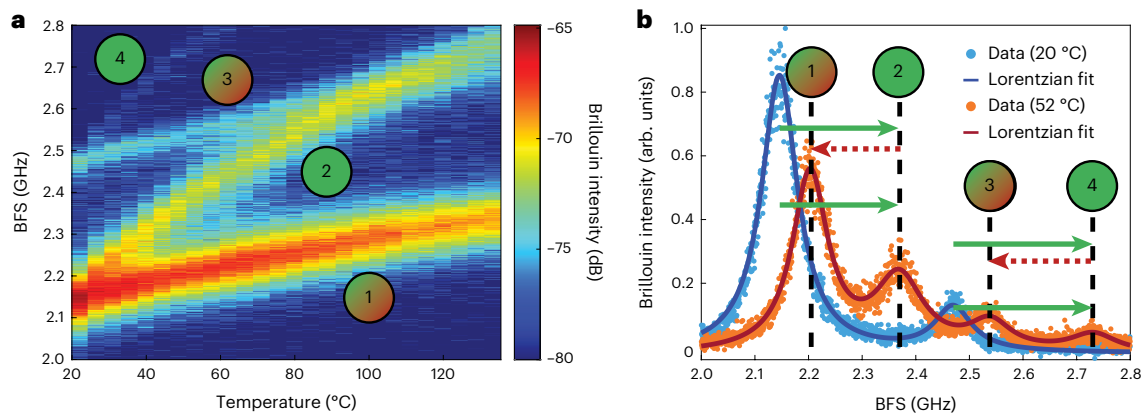


Fig. 2 | Explanation of the observed splitting in integrated Brillouin measurements. **a**, Map of SBS response to partial heating. A splitting of the optical peaks related to the first (second) acoustic mode into two peaks, namely, 1 and 2 (3 and 4), is observed. **b**, Global influence of pressure (upshift, green)

and local influence of temperature (downshift, red) act inversely on the BFS. Although pressure acts on all the peaks, only peaks 1 and 3 are directly influenced by temperature. The spectra match a multi-Lorentzian fit.

create a position-dependent map of the BFS. The resolution and sensing range are governed by the modulation frequency $f_m = 699$ kHz and the modulation bandwidth $\Delta f = 47$ GHz, using

$$\Delta z = \frac{\Delta v_B v_g}{2\pi f_m \Delta f} \quad (3)$$

This yields a resolution of $\Delta z = 6.4$ cm and sensing distance $d_m = 146$ m for a Brillouin gain bandwidth of $\Delta v_B = 65$ MHz, and a group velocity of $v_g = c/n$ with an assumed refractive index of $n = 1.47$ arising from the simulations in ‘Spatially resolved Brillouin–Mandelstam analysis’ section. Due to the longer measurement times of the distributed approach and to reduce spontaneous scattering, shorter fibres of $L = (0.60 \pm 0.05)$ m are used in this section.

Similar to previous measurements, we heat several fractions of the fibre and record the BFS response. Figure 3b,e shows the typical results, with either the half at the incoupling of the probe (Fig. 3b) or half at the incoupling of the pump (Fig. 3e) heated to 80 °C. The shaded parts denote the SMF and ultrahigh-numerical-aperture (UHNA) fibre. The SMF response at these positions is not shown, due to the BFS of $\nu_B = 10.8$ GHz. The dashed white box denotes the region that is heated; the pump direction is always towards the right side of the figure. Calibration measurements reveal a room-temperature BFS of $\nu_B = 2.2$ GHz, in agreement with the integrated data. In contrast to the integrated measurements, only the dominant SBS mode is visible, due to the reduced signal-to-noise ratio of the distributed approach. This is caused by the reduced measurement length and the corresponding exponentially smaller gain. Furthermore, all the measurements exhibit a strong asymmetric background, which is a common feature for direct-frequency-modulated BOCDA⁴¹ and arises from the non-instantaneous amplitude response of the frequency-modulated laser source. To treat this, we conduct numerical simulations for the Brillouin gain following other work^{41,42} (Fig. 3c,f). Neglecting the pump loss inside the fibre, the simulations clearly reproduce the experimental data. The simulations retrieve the initial, undisturbed Brillouin gain distribution (Fig. 3d,g). Additionally, in the simulations, we also suppress the correlation beat noise, which is independent of the laser source. We find that the BFS of the heated regions (cancelling local T and global p influence) is steady at $\nu_B = 2.2$ GHz for all the temperatures, whereas the BFS of the non-heated regions (global p influence only) is upshifted. This is in agreement with the findings from ‘Integrated Brillouin–Mandelstam analysis’ section and confirms our theory of local temperature and global pressure influence in the fibre.

Extreme thermodynamic regimes

As stated in equation (2), the pressure variation inside the fibre can be achieved using partial heating of the waveguide as an indirect method of control. To validate this assumption, the fibre is heated along different fractions and the BFS of peaks 1 and 2 are measured. Peak 1 is dependent on temperature and pressure, whereas peak 2 is only dependent on pressure inside the capillary. In Fig. 4a, the BFS of peak 2 is plotted against the pressure change. The dominating uncertainty of the data points in Fig. 4a is caused by the uncertainty in the heated length. The absolute value of the BFS differs from Fig. 2 because of different sample parameters (2.100 μm diameter instead of 1.125 μm diameter and 2 m length). The overlap for the different heated fractions indicates that the pressure can be tuned independent of the temperature by changing the length of the heated fraction of the capillary. We then complete this picture by including peak 1, which is dependent on the pressure as well as temperature (Fig. 4b). With the full understanding of the pressure and temperature dynamics using equation (1), we are able to tailor the BFS of the fibre over a large range of almost 1.00 GHz (0.97 GHz). This is an unprecedented tunability of more than 40% of the initial value, using only fractional heating with a standard hotplate, offering a tenfold enhancement compared with the temperature tunability of the standard solid-core SMF⁴³. This large tunability in combination with the high gain of our system is highly interesting for optical fibre sensing and microwave photonics applications, such as highly tunable notch filters based on SBS⁴⁴.

In the next step, the fibre is cooled to temperatures below 5 °C (Fig. 4c) resulting in a pressure reduction. In this measurement, most of the fibre is located on a Peltier element except for a short section that is attached on a hotplate. We, therefore, use peak 1, which is influenced by both temperature and pressure. Initially, the fibre is fully filled and thus follows isochoric cooling, and therefore, during cooling down, it shows the expected decrease in the BFS. When the inside of the capillary reaches the vapour pressure of CS_2 (ref. 45), the BFS decrease continues with a steady slope from the positive- to the negative-pressure regime. The latter state may seem less intuitive as one might expect the pressure to be always positive. However, as previous works show, a liquid in tight confinement, such as capillaries or micropores, can be stretched due to adhesion to the vessel boundaries, opening a new thermodynamic metastable regime^{29,30}. In this case, the liquid column is completely filled and the attractive forces between the molecules (cohesion) lead to an inner tension that is expressed as a negative pressure as soon as the system is cooled below the temperature where it would reach vapour pressure. Under this condition,

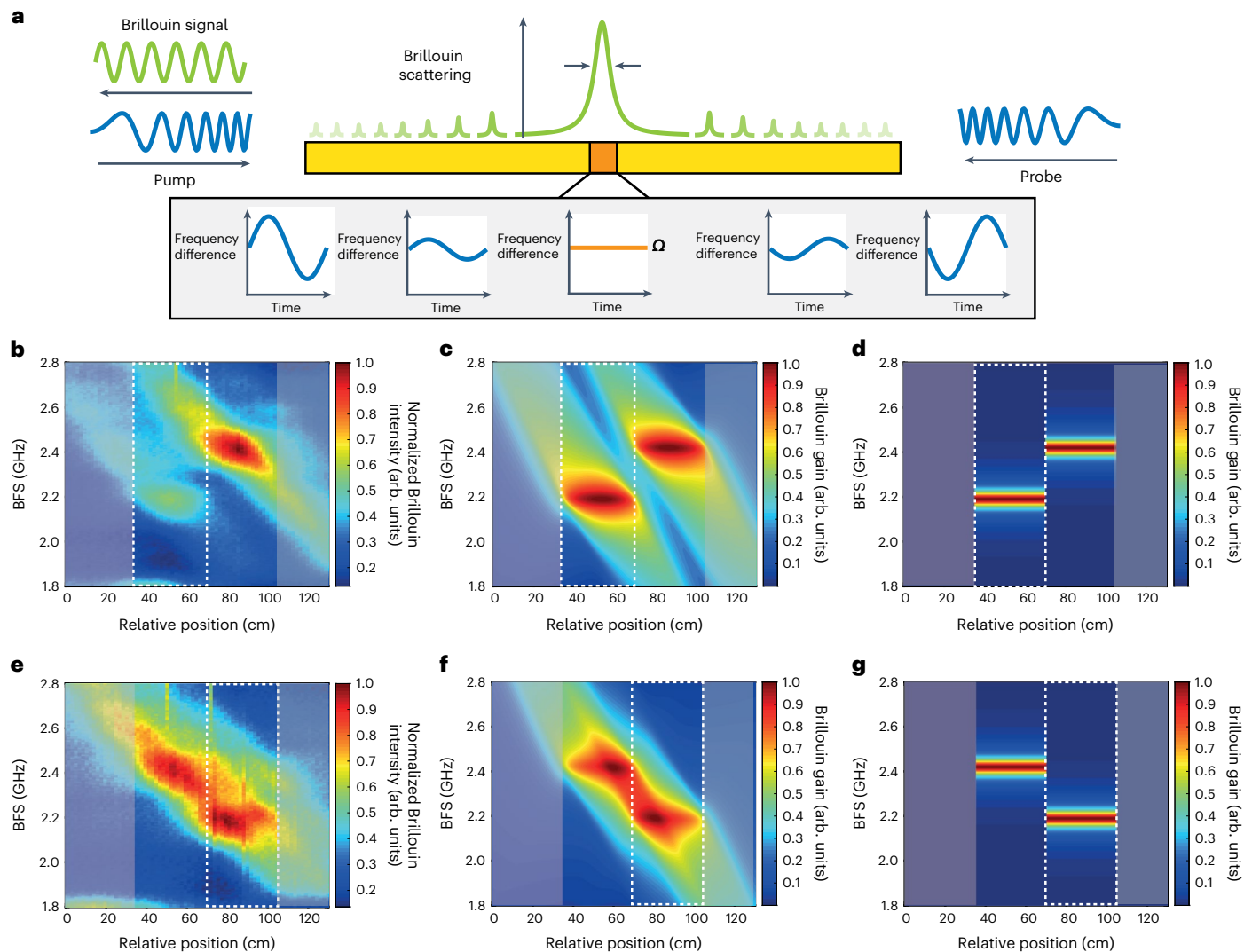


Fig. 3 | Distributed Brillouin measurements. **a**, Scheme of BOCDA. A frequency-modulated, counterpropagating pump and probe wave is launched into the FUT, causing a time- and position-dependent frequency beating. Only at specific correlation positions, the acoustic wave is stimulated and continuously emitted, leading to a continuous-wave, localized Brillouin response. **b, e**, Position-resolved measurement of BFS in partially heated LiCOF; the Brillouin intensity is colour

coded. The heated length is denoted by the dashed white box. The grey-shaded area denotes the system parts of the SMF. The pump direction is from the right. BFS in the non-heated part is upshifted compared with the heated part by approximately $\Delta\nu = 200$ MHz. **c, f**, Numerical simulations of the heated LiCOF BFS response. **d, g**, Initial Brillouin gain distribution retrieved from simulations.

the energetically more favourable phase separation (isobaric state) is suppressed by the attractive cohesion force between the molecules⁴⁶. This metastable state of the liquid column remains intact until an inhomogeneity in the system or a fluctuation of the environment leads to nucleation (bubble formation). Here, as soon as a small perturbation is present, the liquid column breaks up and a liquid–gas interface forms that transfers the system into an isobaric state. The gas phase then expands until the vapour pressure and cohesive forces are in balance again. The metastability of this particular thermodynamic regime is described by the classical nucleation theory⁴⁷, after which an energy barrier must be overcome to break the balance between the forces, eventually leading to homogeneous nucleation. In the experiment, this statistical process is usually triggered by perturbations in the liquid or the experimental system²⁹, which is called heterogeneous nucleation. Additionally, it was shown⁴⁸ that the smaller the capillary, the lower the pressure can get at which heterogeneous nucleation occurs. In our case, the small volume of CS₂, high quality of the capillaries and high mechanical strength of the splices allowed to access negative

pressures of less than -300 bar following equation (2) without homogeneous nucleation.

To initiate nucleation in a controlled way, a small fraction at the end of the fibre is heated above the boiling point of CS₂. At this point, the transmission of the sample is lost, confirming the breakup of the liquid column and thus the onset of the isobaric regime. Furthermore, a strong jump in BFS is visible, caused by the sudden pressure change from large negative pressure to the vapour pressure of CS₂ inherent with nucleation. Next, the liquid is heated in the isobaric regime. The liquid expands with increasing temperature without relevant pressure influence on the BFS⁴⁵. This leads to a large negative slope of the BFS of -7.5 MHz °C⁻¹ (Fig. 4c, red curve), which is a more than sevenfold enhancement compared with standard SMF (0.95 MHz °C⁻¹) (ref. 43). The BFS decreases continuously with a linear behaviour until it reaches the recombination point of 28.7 °C. Here the transmission of the sample is restored as the bubble is closing again. The fibre transitions back from the isobaric to isochoric regime, which are indistinguishable at the recombination point. The exact temperature of the recombination

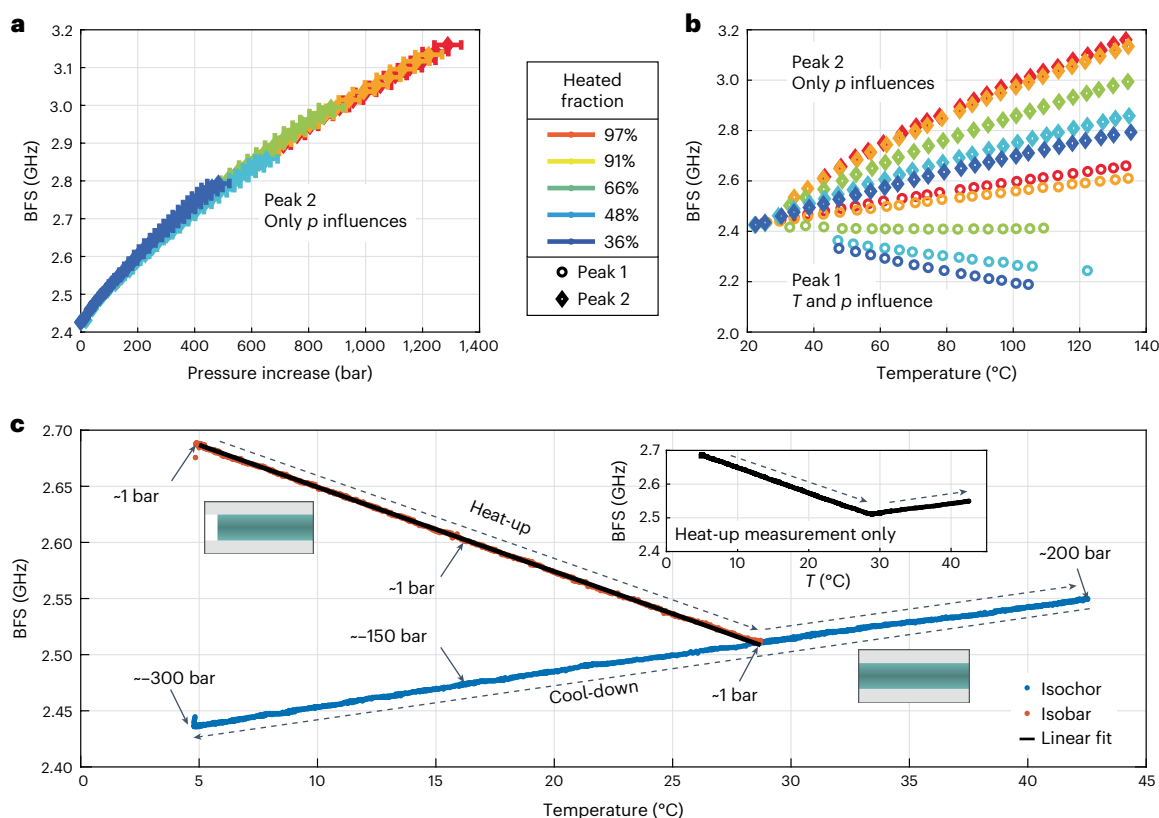


Fig. 4 | Thermodynamic control of stimulated Brillouin scattering (sample with 2.1 μm diameter and 2 m length). **a**, BFS of peak 2 over relative pressure increase for differently long heated fractions of the fibre. **b**, Thermodynamic control of BFS of peaks 1 and 2, which originate from the same resonance, by almost 1.00 GHz (0.97 GHz), changing the temperature and pressure inside the fibre core. **c**, BFS of peak 1 is observed in the isobaric (red curve) and isochoric (blue curve) regime by first cooling down the LiCOF followed by switching to

the isobaric regime by cavitation due to local heating and finally heating up the LiCOF again above the recombination point. In the isobaric regime, we find a large slope of $-7.5 \text{ MHz } ^\circ\text{C}^{-1}$. In the isochoric regime, negative pressures are achieved down to -300 bar. In the inset, the heating-up data are shown, revealing continuous switching from the isobaric to isochoric regimes at around 28°C . The anomaly at around 5°C is due to the initiated cavitation. Supplementary Fig. 2 shows a p - T diagram.

point depends on the filling ratio of the fibre as well as the ratio of the heated to cooled length. For temperatures above this recombination point, the behaviour is described in ‘Integrated Brillouin–Mandelstam analysis’ section.

Conclusion

In summary, we have investigated extensive positive- and negative-pressure regimes in the isobaric and isochoric liquid states of CS_2 with the help of integrated and spatially resolved Brillouin–Mandelstam scattering experiments in fully sealed CS_2 -filled capillary fibres. Pressures of more than 1,000 bar and less than -300 bar were reached, which enables extraordinary control of the Brillouin response with a record tunability of 40% using only a few nanolitres of sample volume of toxic and volatile liquid CS_2 . Distributed Brillouin measurements with centimetre spatial resolution allowed us to experimentally distinguish the local response of temperature changes and the global response of different pressure values. In the isobaric state, we were able to observe the purely temperature-related BFS change of $-7.5 \text{ MHz } ^\circ\text{C}^{-1}$.

In contrast to previous studies^{24,49}, our work opens entirely new optoacoustic insights into the thermodynamic properties of a liquid. Backward SBS provides unique features such as being able to measure in the isobaric regime where no optical transmission is possible and to provide a spatially resolved measurement of the refractive index and sound velocity.

From a materials science point of view, our approach is suitable to access states of matter at conditions that are beyond those

commonly reached, one example being unexplored points in phase diagrams. Some phase transitions that can typically only be seen using invasive approaches might be accessible when studying optoacoustics in fully sealed LiCOFs. Moreover, it can be used to determine difficult-to-measure material constants such as the piezo-optic coefficients¹¹, which are hard to determine otherwise.

This work also marks the successful integration of LiCOF in a fully fibre-based circuitry, opening up an extended application area for fibre optics—the investigation of matter under unexplored conditions of pressure and temperature. The fully sealed fibre system—the overall embedding of the liquid sample into a reproducible micrometre compartment—enables operation in a closed thermodynamic system at the lowest experimental complexity. It enables the use of volatile and toxic liquids in scarce quantities of material. The cleanliness, nanometre-scale size of the core and the reproducibility and cleanliness of the fibre samples preventing organic contamination at the capillary’s inner wall lead to a very reliable and immaculate environment. The approach is also transferable to other fibre types, such as selectively filled air-clad fibres⁵⁰ and is thus principally extendable to liquids with a lower index than silica, such as water.

Our results might, moreover, pave the way for a future generation of liquid-core Brillouin photonics, tailorable by thermodynamic parameters. Consequently, example applications are highly sensitive fibre-based monitoring devices, all-optical switching via nonlinear optical interaction, controlled nanolitre chemistry and widely tunable radio-frequency applications.

Online content

Any methods, additional references, Nature Portfolio reporting summaries, source data, extended data, supplementary information, acknowledgements, peer review information; details of author contributions and competing interests; and statements of data and code availability are available at <https://doi.org/10.1038/s41567-023-02205-1>.

References

- Fortov, V. E. & Lomonosov, I. V. Thermodynamics of extreme states of matter. *Pure Appl. Chem.* **69**, 893–904 (1997).
- Yoon, T. J. et al. Thermodynamics, dynamics, and structure of supercritical water at extreme conditions. *Phys. Chem. Chem. Phys.* **22**, 16051–16062 (2020).
- Pockman, W. T., Sperry, J. S. & O’Leary, J. W. Sustained and significant negative water pressure in xylem. *Nature* **378**, 715–716 (1995).
- Scholander, P. F., Hargens, A. R. & Miller, S. L. Negative pressure in the interstitial fluid of animals: fluid tensions are spectacular in plants; in animals they are elusively small, but just as vital. *Science* **161**, 321–328 (1968).
- Zobeiry, N. & Duffner, C. Measuring the negative pressure during processing of advanced composites. *Compos. Struct.* **203**, 11–17 (2018).
- El Mekki Azouzi, M., Ramboz, C., Lenain, Jean-F. & Caupin, F. A coherent picture of water at extreme negative pressure. *Nat. Phys.* **9**, 38–41 (2013).
- Holten, V. et al. Compressibility anomalies in stretched water and their interplay with density anomalies. *J. Phys. Chem. Lett.* **8**, 5519–5522 (2017).
- Carey, D. M. & Korenowski, G. M. Measurement of the Raman spectrum of liquid water. *J. Chem. Phys.* **108**, 2669–2675 (1998).
- Bhattacharya, J. C. Refractive index measurement. *Opt. Laser Technol.* **19**, 29–32 (1987).
- Schunk, G. et al. Identifying modes of large whispering-gallery mode resonators from the spectrum and emission pattern. *Opt. Express* **22**, 30795–30806 (2014).
- Pumpe, S., Chemnitz, M., Kobelke, J. & Schmidt, M. A. Monolithic optofluidic mode coupler for broadband thermo- and piezo-optical characterization of liquids. *Opt. Express* **25**, 22932–22946 (2017).
- Antman, Y., Clain, A., London, Y. & Zadok, A. Optomechanical sensing of liquids outside standard fibers using forward stimulated Brillouin scattering. *Optica* **3**, 510–516 (2016).
- Marczak, W. Water as a standard in the measurements of speed of sound in liquids. *J. Acoust. Soc. Am.* **102**, 2776–2779 (1997).
- Zha, Chang-S., Hemley, R. J., Mao, Ho-k, Duffy, T. S. & Meade, C. Acoustic velocities and refractive index of SiO₂ glass to 57.5 GPa by Brillouin scattering. *Phys. Rev. B* **50**, 13105 (1994).
- Brewer, R. G. & Rieckhoff, K. E. Stimulated Brillouin scattering in liquids. *Phys. Rev. Lett.* **13**, 334 (1964).
- Hagenlocker, E. E. & Rado, W. G. Stimulated Brillouin and Raman scattering in gases. *Appl. Phys. Lett.* **7**, 236–238 (1965).
- Kobyakov, A., Sauer, M. & Chowdhury, D. Stimulated Brillouin scattering in optical fibers. *Adv. Opt. Photon.* **2**, 1–59 (2010).
- Zarifi, A. et al. Wide-range optical carrier recovery via broadened Brillouin filters. *Opt. Lett.* **46**, 166–169 (2021).
- Santagiustina, M., Chin, S., Primerov, N., Ursini, L. & Thévenaz, L. All-optical signal processing using dynamic Brillouin gratings. *Sci. Rep.* **3**, 1594 (2013).
- Stiller, B. et al. Coherently refreshing hypersonic phonons for light storage. *Optica* **7**, 492–497 (2020).
- Merklein, M., Stiller, B., Vu, K., Madden, S. J. & Eggleton, B. J. A chip-integrated coherent photonic-phononic memory. *Nat. Commun.* **8**, 574 (2017).
- Zadok, A. et al. Random-access distributed fiber sensing. *Laser Photon. Rev.* **6**, L1–L5 (2012).
- Chemnitz, M. et al. Thermodynamic control of soliton dynamics in liquid-core fibers. *Optica* **5**, 695–703 (2018).
- Kieu, K., Churin, D., Schneebeli, L., Norwood, R. A. & Peyghambarian, N. Brillouin lasing in integrated liquid-core optical fibers. *Opt. Lett.* **38**, 543–545 (2013).
- H. Smith, J., M. Peterson, L., H. Rank, D. & A. Wiggins, T. Hypersound speeds in carbon disulfide, acetone, and benzene at high pressure. *J. Acoust. Soc. Am.* **55**, 785–789 (1974).
- Chemnitz, M. et al. Towards telecom-compatible liquid-core fibers for low-power nonlinear signal processing. In *Novel Optical Materials and Applications NoW3C.6* (Optical Society of America, 2021).
- Monfared, Y. E. & Ponomarenko, S. A. Slow light generation via stimulated Brillouin scattering in liquid-filled photonic crystal fibers. *Optik* **127**, 5800–5805 (2016).
- Imre, A., Martínás, K. & Rebelo, L. P. N. Thermodynamics of negative pressures in liquids. *J. Non-Equilib. Thermodyn.* **23**, 351–375 (1998).
- Caupin, F. & Herbert, E. Cavitation in water: a review. *C. R. Phys.* **7**, 1000–1017 (2006).
- Zheng, Q., Durben, D. J., Wolf, G. H. & Angell, C. A. Liquids at large negative pressures: water at the homogeneous nucleation limit. *Science* **254**, 829–832 (1991).
- Wolff, C., Smith, M. J. A., Stiller, B. & Poulton, C. G. Brillouin scattering—theory and experiment: tutorial. *J. Opt. Soc. Am. B* **38**, 1243–1269 (2021).
- Hartog, A. H. *An Introduction to Distributed Optical Fibre Sensors* (CRC Press, 2017).
- Eastman, D. P., Hollinger, A., Kenemuth, J. & Rank, D. H. Temperature coefficient of hypersonic sound and relaxation parameters for some liquids. *J. Chem. Phys.* **50**, 1567–1581 (1969).
- Haynes, W. M. (ed) *CRC Handbook of Chemistry and Physics: A Ready-Reference Book of Chemical and Physical Data* (CRC Press, 2016).
- Kalogerakis, K. S., Blehm, B. H., Forman, R. E., Jirauschek, C. & Faris, G. W. Stimulated Rayleigh and Brillouin scattering in a supercritical fluid. *J. Opt. Soc. Am. B* **24**, 2040–2045 (2007).
- Behunin, R. O., Ou, Yi-H. & Kieu, K. Spontaneous forward Brillouin scattering in carbon disulfide. *Phys. Rev. A* **99**, 063826 (2019).
- Lanticq, V. et al. Self-referenced and single-ended method to measure Brillouin gain in monomode optical fibers. *Opt. Lett.* **34**, 1018–1020 (2009).
- Nikles, M., Thevenaz, L. & Robert, P. A. Brillouin gain spectrum characterization in single-mode optical fibers. *J. Light. Technol.* **15**, 1842–1851 (1997).
- Hotate, K. & Hasegawa, T. Measurement of Brillouin gain spectrum distribution along an optical fiber using a correlation-based technique—proposal, experiment and simulation—. *IEICE Trans. Electron.* **83**, 405–412 (2000).
- Zarifi, A. et al. Brillouin spectroscopy of a hybrid silicon-chalcogenide waveguide with geometrical variations. *Opt. Lett.* **43**, 3493–3496 (2018).
- Song, K. Y. & Choi, J. H. Measurement error induced by the power-frequency delay of the light source in optical correlation-domain distributed Brillouin sensors. *Opt. Lett.* **43**, 5078–5081 (2018).
- Yamauchi, T. & Hotate, K. Performance evaluation of Brillouin optical correlation domain analysis for fiber optic distributed strain sensing by numerical simulation. In *Fiber Optic Sensor Technology and Applications III* **5589**, 164–174 (International Society for Optics and Photonics, 2004).

43. Thévenaz, L. Brillouin distributed time-domain sensing in optical fibers: state of the art and perspectives. *Front. Optoelectron. China* **3**, 13–21 (2010).
44. Pant, R. et al. On-chip stimulated Brillouin scattering for microwave signal processing and generation. *Laser Photon. Rev.* **8**, 653–666 (2014).
45. Waddington, G., Smith, J. C., Williamson, K. D. & Scott, D. W. Carbon disulfide as a reference substance for vapor-flow calorimetry; the chemical thermodynamic properties. *J. Phys. Chem.* **66**, 1074–1077 (1962).
46. Davitt, K., Rolley, E., Caupin, F., Arvengas, A. & Balibar, S. Equation of state of water under negative pressure. *J. Chem. Phys.* **133**, 174507 (2010).
47. Debenedetti, P. G. *Metastable Liquids: Concepts and Principles* (Princeton Univ. Press, 1996).
48. Brereton, G. J., Crilly, R. J. & Spears, J. R. Nucleation in small capillary tubes. *Chem. Phys.* **230**, 253–265 (1998).
49. Fanjoux, G., Margueron, S., Beugnot, Jean-C. & Sylvestre, T. Supercontinuum generation by stimulated Raman–Kerr scattering in a liquid-core optical fiber. *J. Opt. Soc. Am. B* **34**, 1677–1683 (2017).
50. Bethge, J. et al. Two-octave supercontinuum generation in a water-filled photonic crystal fiber. *Opt. Express* **18**, 6230–6240 (2010).

Publisher's note Springer Nature remains neutral with regard to jurisdictional claims in published maps and institutional affiliations.

Open Access This article is licensed under a Creative Commons Attribution 4.0 International License, which permits use, sharing, adaptation, distribution and reproduction in any medium or format, as long as you give appropriate credit to the original author(s) and the source, provide a link to the Creative Commons license, and indicate if changes were made. The images or other third party material in this article are included in the article's Creative Commons license, unless indicated otherwise in a credit line to the material. If material is not included in the article's Creative Commons license and your intended use is not permitted by statutory regulation or exceeds the permitted use, you will need to obtain permission directly from the copyright holder. To view a copy of this license, visit <http://creativecommons.org/licenses/by/4.0/>.

© The Author(s) 2023

Methods

LiCOF Sample

The LiCOF sample is depicted in Fig. 1c. Liquid CS₂ is sealed within a SiO₂ glass capillary by spliced UHNA fibres and standard SMFs to allow a simple implementation into the setup. Different samples were used in the experiments, which have slightly different parameters due to fabrication reasons. The core size of the samples used in this work is 1.125 μm ($V = 1.51$, thus optically single mode at $\lambda = 1,549$ nm) and 2.100 μm ($V = 2.82$, thus optically multimode at $\lambda = 1,549$ nm). The length of the LiCOF part is between 0.6 and 2.0 m. Unless otherwise specified, a length of $L = 2.00 \pm 0.05$ m and a core diameter of 1.125 μm are the parameters of the samples employed in this study. Not only is the LiCOF optically guiding but also acoustically: as the longitudinal velocity of sound in the core ($-1,242$ m s⁻¹ (ref. 25)) is less than the velocity of shear wave in silica cladding ($-3,765$ m s⁻¹), all the acoustic-mode fields in the cladding are evanescent and the acoustic mode is, therefore, guided by total internal reflection. More information on the samples can be found elsewhere⁵¹.

For all the measurements shown in this Article, except for the ones explicitly noted in ‘Extreme thermodynamic regimes’ section, the fibre is in an isochor state, meaning that the liquid is fully filling the fibre (Fig. 1c). This is confirmed by the fact that the fibre has transmission at all times except for the measurement explicitly stated in ‘Extreme thermodynamic regimes’ section, which is plotted in Fig. 4c (red). Due to the full sealing of the fibre, CS₂ is always in a liquid state, as the sealing, confinement and pressure increase prevents phase changes (as explained elsewhere⁵¹).

The influence of pressure and temperature on the geometry of the sample is negligible: due to the rigid nature of the glass and small capillary size, changes in the diameter are two orders of magnitude smaller than the diameter itself (Supplementary Section 3).

Setup for integrated SBS measurements

The simplified setup for the integrated SBS measurements is presented in Extended Data Fig. 1. A laser at wavelength $\lambda = 1,549$ nm is split up into a local oscillator part and a pump part. The pump part is modulated via a Mach–Zehnder modulator into 30 ns pulses and subsequently amplified by an erbium-doped fibre amplifier. To suppress the amplified spontaneous emission, a 1 nm optical bandpass filter is used. The final pump power is measured using a power meter. Via an optical circulator, the pump light is sent into the LiCOF, where backscattered SBS is created by employing thermal phonons as the seed. Although the transmitted pump is dumped, the backscattered SBS is guided onto a high-frequency photodiode via the circulator. By mixing the SBS signal with the previously detached local oscillator, a heterodyne measurement is performed on the electrical spectrum analyser. Before the Mach–Zehnder modulator and before mixing, the polarization is controlled via a fibre-integrated polarization controller to maximize the transmission and beating amplitude, respectively.

Details on integrated SBS measurements and simulations

The backward-integrated SBS measurements are performed at $\lambda = 1,549$ nm using an optically heterodyne measurement technique and an electronic spectrum analyser, as described in ‘Setup for integrated SBS measurements’ section. The linewidth is extracted from seeded SBS measurements at the same wavelength with a lock-in detection for a modulated pump. As the fibre has a core diameter of 1.125 μm, one finds a V number of 1.510, indicating optical single-mode operation (that is, $V < 2.405$). For numerical simulations, COMSOL Multiphysics (version 5.6) is employed to calculate the optoacoustic overlap between the optical fundamental mode and the first three radially symmetric longitudinal-pressure acoustic modes (L_{01} , L_{02} and L_{03}). Here we follow the theoretical work from another study¹⁷. We assumed a constant linewidth of 65 MHz for all the modes obtained from the

measurements. To match the simulations with the measurements, free parameters in the model are fitted. The absolute frequency position is influenced by the unknown initial pressure assuming a linear relation between the pressure and BFS. The relative frequency position is matched by fitting the fibre diameter and is found to be 1.125 μm. To fit the gain, the thermal Stokes seed as well as global gain are fitted. Each measurement is performed once the fibre–heater system has reached thermodynamic equilibrium, which takes about five to ten minutes after changing the temperature.

Details on BOFDA measurements in LiCOF

The complete BOFDA setup is presented in Extended Data Fig. 2. The local acoustic response is created through frequency modulation of the master laser source with modulation frequency $f_m = 699$ kHz and modulation bandwidth $\Delta f = 47$ GHz resulting in a resolution of $\Delta z = 5.9$ cm. Due to the repetitive nature of the correlation approach, the sensing distance is limited by $d_m = v_g/2f_m$ with group velocity v_g . This modulation is realized using a directly current-modulated distributed fibre Bragg laser. The modulation is generated using an external radio-frequency source. After passing an isolator, the signal is split 50:50 into a pump and probe beam. The probe is passed through a single-sideband modulator, shifting it downwards by the Brillouin frequency ν_B . After amplification through an erbium-doped fibre amplifier, 1% is split off for power or spectral monitoring. The signal is filtered using a narrow-band bandpass and afterwards, the polarization is scrambled with a frequency of $f_{rand} = 700$ kHz. After passing a delay, it is launched into the fibre under test (FUT). The seed input is monitored using a second tap-off. The pump beam is modulated with the lock-in frequency of $f_{lock} = 100$ kHz. Then, it is amplified using a second erbium-doped fibre amplifier. After polarization adjustment, the pump is launched into the FUT using a fibre-integrated optical circulator. Again, the power is monitored using a 1% tap-off. The backscattered Brillouin signal is detected on a photodiode and demodulated through the lock-in amplifier. The signal is monitored at an oscilloscope with a temporal reference from the single-sideband modulation frequency to retrieve the spectral information.

For our numerical simulations, we follow the frequency-domain approach⁴² in combination with the non-instantaneous amplitude-to-frequency response approach⁴¹. The discrete beat spectrum $S_B(z, f)$ of pump and probe is calculated and convoluted with the analytical amplitude beat spectrum $S_A(z, f)$ resulting from the non-instantaneous amplitude-to-frequency response. The resulting beat spectrum is finally convoluted with the Brillouin gain spectrum $g_B(f)$ to retrieve the position-dependent normalized Brillouin gain $g_B(z, f)$. Due to the small resolution of $\Delta z = 6.4$ cm, the distributed Brillouin signal can be seen as a Brillouin signal in the small-gain limit.

Data availability

Source data are available for this paper. All other data that support the plots within this paper and other findings of this study are available from the corresponding author upon reasonable request.

References

- Chemnitz, M. Hybrid soliton dynamics in liquid-core fibres. *Nat. Commun.* **8**, 42 (2017).

Acknowledgements

We acknowledge our co-workers D. Walter, F. Sedlmeier, A. Zarifi, X. Zeng, S. Becker and A. Tuniz for valuable discussions, and L. Meier, O. Bittel, R. Gall, M. Schwab and A. Wambsganß for support with the custom-built mechanics and electronics of the systems. B.S. acknowledges funding from the Max Planck Society through the Independent Max Planck Research Group scheme. M.C. acknowledges funding from the Banting Foundation (Canada), the FRQNT through

the PBEEE Fellowship and the Carl Zeiss Stiftung (Nexus program). C.G.P. acknowledges funding from the ARC Discovery Project DP200101893.

Author contributions

B.S., M.C. and M.A.S. conceived the idea. A.G., A.P. and D.D. performed the experiments and analysed the data. S.J. fabricated the sample. All authors discussed the results and worked on their interpretation. A.G., A.P., M.C., C.G.P., M.A.S. and B.S. wrote the paper with input from all authors. M.C., C.M., M.A.S. and B.S. supervised the project.

Funding

Open access funding provided by Max Planck Society.

Competing interests

The authors declare no competing interests.

Additional information

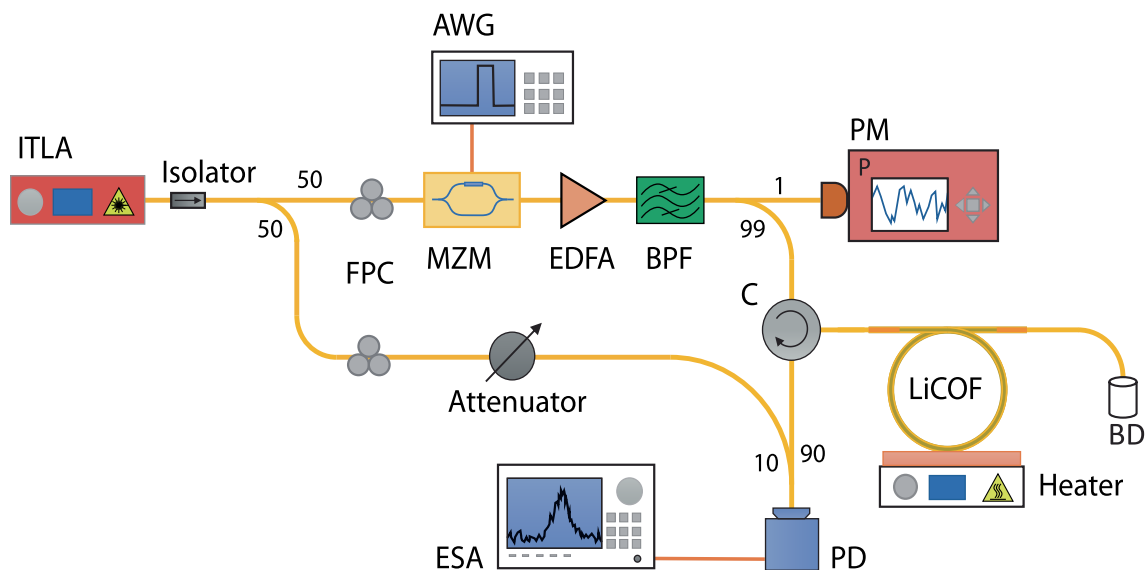
Extended data is available for this paper at <https://doi.org/10.1038/s41567-023-02205-1>.

Supplementary information The online version contains supplementary material available at <https://doi.org/10.1038/s41567-023-02205-1>.

Correspondence and requests for materials should be addressed to Birgit Stiller.

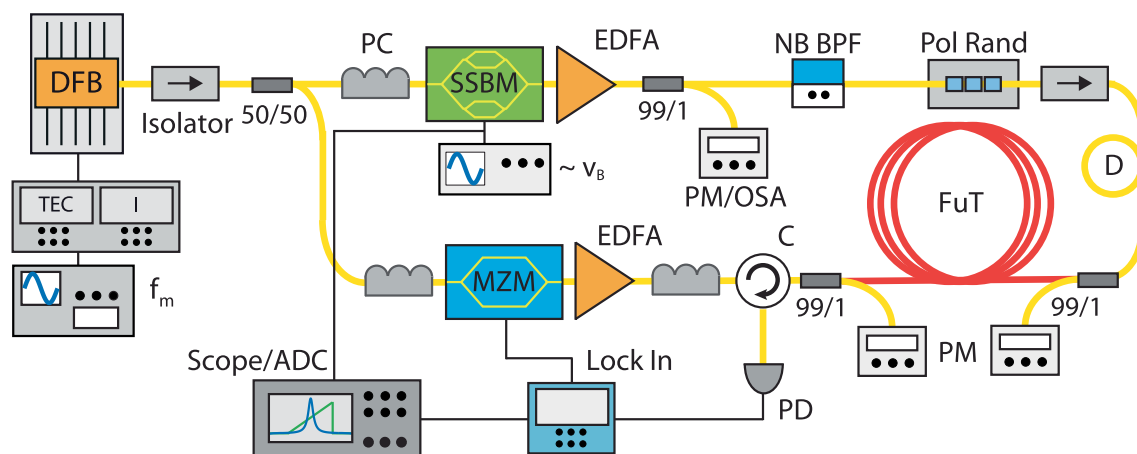
Peer review information *Nature Physics* thanks Irina Kabakova and the other, anonymous, reviewer(s) for their contribution to the peer review of this work.

Reprints and permissions information is available at www.nature.com/reprints.



Extended Data Fig. 1 | Schematic sketch of integrated SBS setup. ITLA: integrated tunable laser assembly, I: laser current controller, Isolator: fibre-integrated optical isolator, FPC: fibre-integrated polarization controller, EDFA: Erbium-doped fibre amplifier, PM: power meter, ESA: electrical spectrum

analyser, MZM: fibre-integrated Mach-Zehnder Modulator, AWG: arbitrary waveform generator, LiCOF: liquid core optical fibre (target), C: fibre-integrated optical circulator, PD: photo diode, heater: electrical heater plate, BD: beam dump, BPF: band-pass filter for ASE suppression.



Extended Data Fig. 2 | Schematic sketch of BOCDA setup. DFB: distributed fibre Bragg laser, TEC: laser temperature controller, I: laser current controller, Isolator: fibre-integrated optical isolator, PC: fibre-integrated polarization controller, f_m : radio-frequency generator for laser current modulation, 50/50: fibre-integrated beamsplitter ratio 50:50, SSBM: fibre-integrated single-sideband modulator, v_B : radio-frequency generator for Brillouin resonance modulation, EDFA: Erbium-doped fibre amplifier, 99/1: fibre-integrated

beamsplitter ratio 99/1, NB BPF: fibre-integrated narrow-band bandpass filter, Pol Rand: fibre-integrated polarization scrambler, PM: power meter, OSA: optical spectrum analyser, D: delay, MZM: fibre-integrated Mach-Zehnder Modulator, FuT: fibre under test (target), C: fibre-integrated optical circulator, PD: photo diode, Lock In: lock-in amplifier, Scope/ADC: oscilloscope or analogue-to-digital-converter.